CHEMISTRY OF MATERIALS

ARTICLE

pubs.acs.org/cm

$Bi_2Ti_2O_7$: It Is Not What You Have Read

J. Roberto Esquivel-Elizondo, Beverly Brooks Hinojosa, and Juan C. Nino*

Department of Materials Science and Engineering, University of Florida, Gainesville, Florida 32611, United States

Supporting Information

ABSTRACT: Coprecipitation synthesis methods followed by microwave sintering techniques were utilized to obtain dense phase pure $Bi_2Ti_2O_7$ polycrystalline ceramic pellets. No evidence of secondary phases was found in the powder or pellets. This maiden achievement allowed for primary thermophysical, crystallographic, and dielectric characterization of this ceramic compound. Density functional theory was used to model the structure of the pyrochlore, from which the theoretical X-ray diffraction pattern was obtained to determine the purity of the experimental compound. Discrepancies among reports in literature regarding the structure, stability, and supposed ferroelectricity of this material are discussed and clarified. A modification to the phase diagram of the $Bi_2O_3-TiO_2$ system is proposed based on the results of the present investigation. In addition, and contrary to prior reports, the dielectric characterization of $Bi_2Ti_2O_7$ reveals a linear dielectric with high permittivity values at room temperature (115 at 500 kHz), and more remarkably, a temperature and frequency dependent dielectric relaxation.

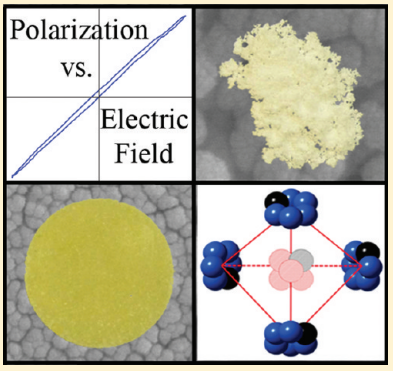

KEYWORDS: pyrochlore, microwave sintering, dielectric relaxation, $Bi_2O_3-TiO_2$ phase diagram, coprecipitation

1. INTRODUCTION

The phase diagram of $Bi_2O_3-TiO_2$ was first published in 1965 by Speranskaya and co-workers,[1] and since then, the bismuth compounds reported there have been extensively studied due to their unique set of properties. Combining the ensuing work by Bruton[2] and Masuda et al.[3] a total of five bismuth titanate compounds have been identified: $Bi_4Ti_3O_{12}$, $Bi_2Ti_4O_{11}$, $Bi_{12}TiO_{20}$, Bi_8TiO_{14}, and $Bi_2Ti_2O_7$.

The well-known Aurivillius phase (layered perovskite-like) $Bi_4Ti_3O_{12}$ is a ferroelectric compound that has been synthesized by different methods such as solid-phase reaction,[4] coprecipitation,[5] and mechanochemical activation.[6] $Bi_2Ti_4O_{11}$ is antiferroelectric at low temperature (α-$Bi_2Ti_4O_{11}$) and transforms into paraelectric (β-$Bi_2Ti_4O_{11}$) at 233 °C.[7] The crystal structure of both phases was studied by Kahlenberg and Böhm[8] who used a flux method to grow single crystals. The optical properties of $Bi_{12}TiO_{20}$ are a subject of much interest and many authors have studied them. The compound has been synthesized by solid state reaction[9] and coprecipitation.[10] Moreover, single crystals have been grown by the Czochralski method.[11,12] The existence of Bi_8TiO_{14} is controversial since it was reported by Masuda et al.[3] but not by Bruton[2] or Lopez-Martinez et al.[13]

The case of the pyrochlore $Bi_2Ti_2O_7$ is different from the previous ones and rather interesting. Even 42 years after Knop et al.[14] attempted to make the compound using the solid state reaction method, it is not possible to say with certainty, the chemical and physical properties of this material due to the large differences within literature. The existence, stability, crystal structure, bulk densification (sintering), and dielectric properties of the pyrochlore, often (wrongfully) reported as ferroelectric,[3,15−19] have been subject of discussion for many years. In the present work, a comprehensive study was carried out in order to clarify these issues concerning the synthesis, crystal structure, thermal stability, sintering, and electrical properties of $Bi_2Ti_2O_7$.

2. EXPERIMENTAL SECTION

2.1. Synthesis. To prepare 0.01 mol of $Bi_2Ti_2O_7$, glacial acetic acid (Alfa Aesar, 99+%), bismuth nitrate pentahydrate (Fisher, certified), ammonium hydroxide (Acros Organics, 28−30% solution of NH_3 in water), and titanium(IV) isopropoxide (Acros Organics, 98+%) were used as starting materials. Bismuth nitrate (0.02 mol) was dissolved in acetic acid (25 mL) after approximately 20 min of stirring. The ammonium hydroxide (33 mL) was kept in a freezer below 0 °C, while the bismuth nitrate was dissolved. Titanium isopropoxide (0.02 mol plus an excess of 23%, which has been found to be the optimum ratio to obtain a pure $Bi_2Ti_2O_7$ phase[20]) was later added to the bismuth nitrate solution followed by 5 min of stirring. The ammonium hydroxide was poured into this mixture (a strongly exothermic reaction) and after vigorous (manual) agitation a white precipitate was formed (the pH of the solution at this point was ~7). The precipitate was filtered, rinsed with abundant water, and dried overnight. Slightly yellow chunks were obtained and were ground with a mortar and a pestle until a homogeneous white fine powder was observed. An alternative method consisted of following the same procedure just described but with the next changes: bismuth subnitrate (Fisher USP, 0.02/5 mol) was used instead of bismuth nitrate, and acetic acid was replaced with nitric acid 35% v/v (Ricca Chemical Company, 40 mL). The rest remained the same (but 40 mL of NH_3OH substituted 33 mL).

A calcination step was carried out at 550 °C for 16 h with a heating and cooling rate of 200 °C/h in a zirconium oxide crucible. The powder was pressed (50 MPa) into pellets of 7 and 13 mm in diameter. The

Received: July 26, 2011
Revised: October 3, 2011
Published: October 25, 2011

pellets were microwave sintered in a ThermWAVE 1.3 furnace using silicon nitride susceptors to attain a heating rate of 80 °C/min and a holding temperature of 1200 °C for 45 min. The samples were ambient cooled to room temperature inside the microwave furnace. For dielectric and polarization vs electric field measurements sintered samples were polished to a 1200 grit (SiC) finish, sonicated in water for 10 min and then electroded with gold (sputter coated) and silver paste. They were then dried overnight at 120 °C. Before the polarization vs electric field tests, the samples were poled at 140 °C under a voltage of 30 kV/cm for 30 min.

2.2. Characterization. X-ray diffraction (XRD) patterns of the pellets (Philips APD 3720, Cu K-alpha source) and powder (INEL CPS 120, Cu K-alpha source) were collected to verify phase purity and the scanning electron microscope (SEM) images were obtained with a field emission JEOL 6335F FEG-SEM. For differential thermal analysis (DTA), 15 mg powder samples were set on a platinum pan in nitrogen atmosphere with a heating rate of 10 °C/min in a Seiko Instruments TGA/DTA 320 SSC/5200 series.

The dielectric measurements were computer controlled with a closed cycle cryogenic workstation (CTI-Cryogenics, Model 22) in the temperature range of −248 to 22 °C and a Delta 9023 oven from 22 to 200 °C. The measurements were conducted during cooling and heating cycle. Since no thermal hysteresis was observed, only the data from the heating cycle are presented here. The polarization-electric field (P-E) loop was measured with a Sawyer−Tower circuit with a sinusoidal wave at 50 Hz.

2.3. Computational Methods. First-principles calculations were performed with Vienna ab initio Simulation Package (VASP),[21−24] a plane-wave density functional theory (DFT) code, using the projector augmented wave (PAW) pseudopotentials provided in the VASP database.[25,26] The Bi(5d, 6s, 6p), O(2s, 2p), and Ti(3s, 3p, 3d, 4s) orbitals were included as the valence electrons. The calculations were performed within the local density approximation (LDA),[27] which is expected to underestimate lattice constants and overestimate the strength of bonding, but has been found to be more accurate than the GGA functionals for many pyrochlores.[28,29] Electronic relaxation was performed with the conjugate gradient (CG) method accelerated using Methfessel−Paxton Fermi-level smearing with a Gaussian width of 0.1 eV.[30] The equilibrium lattice constant identified as 10.34 Å in previous DFT simulations[28] was reevaluated by performing several optimizations at different volumes. The total energy as a function of the structure's volume was examined and the lowest energy (most thermodynamically stable) structure corresponded to a lattice parameter of 10.335 ± 0.005 Å. Recent work examined the affect of relaxing the shape of $Bi_2Ti_2O_7$ and found the cubic system with atomic displacement to be the most favorable structure.[31] Therefore, the calculations were performed with the shape fixed and at the new equilibrium volume, while the atoms were optimized until the forces were less than 0.01 eV/Å. A plane wave cutoff energy of 400 eV was used along with a 4 × 4 × 4 Monkhorst-Pack[32] mesh, resulting in 10 irreducible *k*-points. Test calculations done with 520 eV cutoff and a 6 × 6 × 6 mesh result in differences less than 0.02 eV/88-atom cell in the total energy, well within the error for the results presented in this paper. Several test calculations were performed to confirm that spin-polarization does not affect any of the results; therefore, all data reported in the paper are without spin-polarization.

Typically, when considering the pyrochlore structure, the $Fd\bar{3}m$ space group (No. 227) in its origin choice 2 (origin at the 16*c* site) is utilized. The ideal high symmetry sites occupied by a pyrochlore ($A_2B_2O_6O'$) are the A cation at 16*c* site (0,0,0), B cation at 16*d* site (1/2,1/2,1/2), O anion at 48*f* site (*x*,1/8, 1/8), and O′ anion at the 8*a* site (1/8, 1/8, 1/8). The two oxygen types are distinguished due to the different symmetry of each site. Based on the atomic displacements obtained in the DFT simulations the relaxed positions for each of the 88 atoms within the unit cell were collectively examined and the Wyckoff positions were assigned.

Table 1. Lattice Parameter of $Bi_2Ti_2O_7$ Calculated by Different Methods and the Atomic Positions Predicted by DFT Simulations for Cubic $Bi_2Ti_2O_7$

a (Å)				10.335 ± 0.005 (DFT)		
				10.335 ± 0.008 (CPS XRD)[a]		
				10.327 ± 0.002 (Le Bail)		
atom	Wyckoff Position	*x*	*y*	*z*	U_{iso}	occupancy
Bi	96*g*	0.015	0.015	0.964	0.001	1/6
Ti	16*d*	1/2	1/2	1/2	0.023	1
O	48*f*	0.431	1/8	1/8	0.010	1
O′	48*f*	0.136	1/8	1/8	0.003	1/6

[a] By a linear extrapolation for curved position-sensitive (CPS) detectors.[40]

The 88 atoms result from the 8 formula units necessary to describe a pyrochlore compound ($A_2B_2O_6O'$) within the $Fd\bar{3}m$ space group by 16 A cations, 16 B cations, 48 O anions and 8 O′ anions. The Crystal Maker software program was used to create all the equivalent positions within the $Fd\bar{3}m$ space group (no. 227) by applying relevant symmetry operations. The theoretical diffraction patterns were generated by Crystal Diffract software program in order to compare the computational results with the experimental X-ray diffraction patterns.

3. RESULTS AND DISCUSSION

3.1. $Bi_2Ti_2O_7$ Structure from DFT Simulation. The bismuth titanate pyrochlore phase has been studied in several computational investigations.[28,33−37] Recent investigations based on first principles have reported lattice instability for the cubic bismuth titanate pyrochlore when considering the atoms on the ideal high symmetry sites, which resulted in lattice distortions converging toward a monoclinic *Cm* or orthorhombic $Pna2_1$ space groups.[33,35,37] However, it is well-known that the Bi within $Bi_2Ti_2O_7$ will displace off the high symmetry positions in the $Fd\bar{3}m$ space group.[28,38,39] When atomic displacements were considered, bismuth titanate was stable within the $Fd\bar{3}m$ space group and no lattice instabilities were found from phonon dispersion calculations.[31]

Early DFT simulations on the $Bi_2Ti_2O_7$ found Bi, Ti, and O′ atoms displaced with various positions identified.[28] Briefly, in these results Bi occupied three positions (96*g*, 96*h*, and 192*i*), O′ occupied the 192*i* centered at (1/8,1/8,1/8), and Ti also occupied the 192*i* position centered at (1/2,1/2,1/2). A recent study focused on expanding these results to examine the symmetry equivalent displacement sites for the Bi cations and a new energetic minimum was found.[31] Phonon dispersion calculations were performed, and no soft modes were seen indicating the stability of the new minimum.[31] By contrast, when the phonon dispersion calculations were completed for the structure reported in ref 28 four soft modes were identified. Given the improved thermodynamics and structure stability of the recently identified minimum from ref 31, this section will focus on characterizing the atomic positions in order to compare with the experimental results reported in the following sections. Therefore, using the fully optimized cubic bismuth titanate pyrochlore with atomic displacements from ref 31, the Wyckoff positions were identified for the Bi, Ti, O, and O′ atoms and are summarized in Table 1. The Bi atoms exclusively occupy the 96*g*(*x*,*x*,*z*) Wyckoff position and result in 6 symmetrically equivalent positions for each of 16 Bi cations. As mentioned above, this

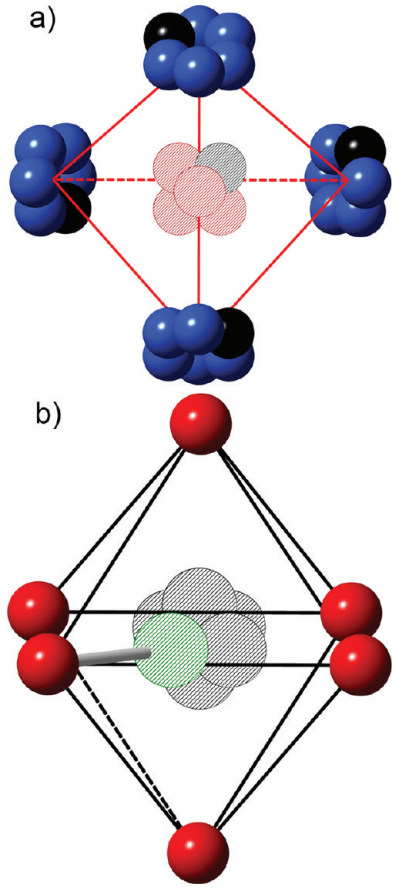

Figure 1. Predicted displacement pattern for the (a) O'Bi_4 tetrahedron with the O' at 48*f* and the Bi at 96*g* and (b) a snapshot of the TiO_6 octahedron with Ti at 96*g* and O at 48*f*. The displacement magnitudes were exaggerated for the O′ and Ti for visual aid.

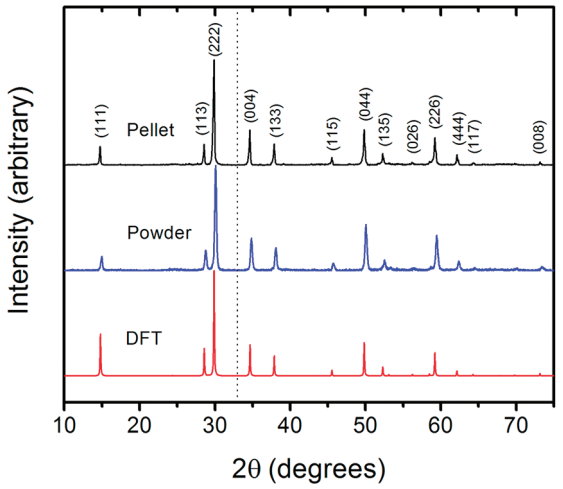

Figure 2. Theoretical (using DFT predicted atomic positions) and experimental (powder and pellet) X-ray diffraction patterns of $Bi_2Ti_2O_7$. For visual aid, a dashed line is included at 33° to illustrate the lack of secondary phases.

displacement was identified in bismuth titanate previously and results in a puckered ring centered on the 16*c*(0,0,0) site.[28,38] The O′ anions exclusively bond to the Bi cations and after optimization occupy the 48*f* position. Previous reports indicated that the O′ anions displace to the 32*e* position[38] or the 192*i* position.[28] The O′ anions within the 48*f* position displace toward the six edges of the O′Bi_4 tetrahedra, as illustrated in Figure 1a. Correlation of the Bi and O′ displacements has been seen by multiple researchers[28,37] and was observed here. One of the actual displacement patterns of the O′ and Bi cations is highlighted in Figure 1a as the black atoms. The O′ anion displaced up and to the right (along the $[0\bar{1}0]$ direction) while the Bi along the horizontal axis exhibited correlated displacement (along the $[0\bar{1}\bar{1}]$ direction).

Remarkably, it is found that the Ti atoms also occupy the 96*g*(*x*,*x*,*z*) Wyckoff position but the resulting 6 equivalent positions are centered around the 16*d*(1/2,1/2,1/2). The 96*g* position for Ti has the Ti atoms displacing with a magnitude of 0.13 Å toward each of the vertices of the TiO_6 octahedra, as seen in Figure 1b. One of the six possible displacement patterns is highlighted in green and results in a shorten Ti−O bond length (distinguished in Figure 1b) of 1.84 Å (versus two bonds at 1.92 Å, two bonds at 2.01, and one bond at 2.08 Å for the other oxygen anions making up the octahedron). The displacement pattern for Ti reported here also differs from the previously reported 192*i* position.[28] For the case of the 192*i* position, the Ti displaced by a smaller magnitude and not directly toward one of the six O atoms within the octahedron. The difference between the two displacement patterns is attributed to the Bi displacement. The details of the Bi occupying the 96*g* or 96*h* position have been discussed previously by Hector and Wiggin[38] and Radosavljevic,[39] respectively. Briefly, when Bi occupies the 96*g* site it displaces directly toward one O atom and simultaneously away from another O atom, resulting in an under-coordinated O atom. It was observed that with the Ti occupying the 96*g* site, the Ti atom displaces toward this under-coordinated O atom. For aid in viewing the displacement pattern, the magnitudes of both the Ti and O′ displacements were exaggerated and the atomic radii were modified for all the atoms.

It is not unexpected for DFT to predict Ti displacement to satisfy the under-coordinated O after Bi displacement. However, DFT captures snapshots of the material without thermal considerations and experimental efforts have not identified static Ti displacement. Therefore, in the absence of experimental evidence, the Ti displacement is reinterpreted as an isotropic displacement about the high symmetry 16*d* site. This isotropic displacement would be evidenced by a broader diffraction peak associated with Ti at the 16*d* site.

With the stability of the $Fd\bar{3}m$ space group confirmed, the lattice parameter optimized, and the atomic positions and thermal parameters identified by DFT (in Table 1), the theoretical X-ray diffraction pattern was generated and it is presented in Figure 2. The theoretical pattern based on the DFT predicted structure is compared with the observed XRD from the experimentally synthesized bismuth titanate in the following section.

3.2. Synthesis of Cubic $Bi_2Ti_2O_7$ Pyrochlore. In 1969, Knop and collaborators,[14] while studying pyrochlore titanates, attempted to make the compound using the solid state reaction method but did not succeed. Instead, they made $Y_{1-x}Bi_xTi_2O_7$ with different compositions and extrapolated the data to give an estimate of the lattice parameter (10.354 Å), but concluded that $Bi_2Ti_2O_7$ was not a cubic pyrochlore. Later in 1977, Shimada et al.[41] claimed the growth of $Bi_2Ti_2O_7$ single crystals which were described as "reddish brown crystals". The structure was simply defined as a face centered-cubic with a unit cell of 20.68 Å.

dx.doi.org/10.1021/cm202154c |*Chem. Mater.* 2011, 23, 4965–4974

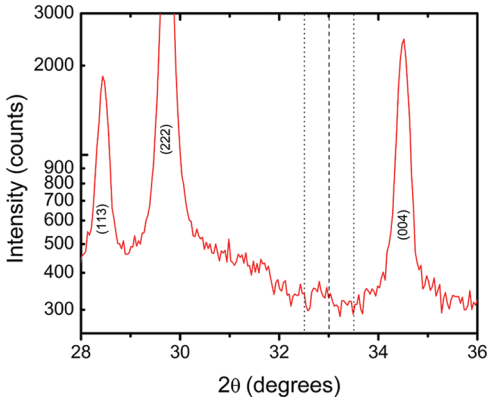

Figure 3. Magnification in logarithmic scale of the XRD pattern around the area where common bismuth titanate impurities (perovskite and monoclinic) would be observed if present. For visual aid, dashed lines are included at 33° ± 0.5 to illustrate the lack of secondary phases.

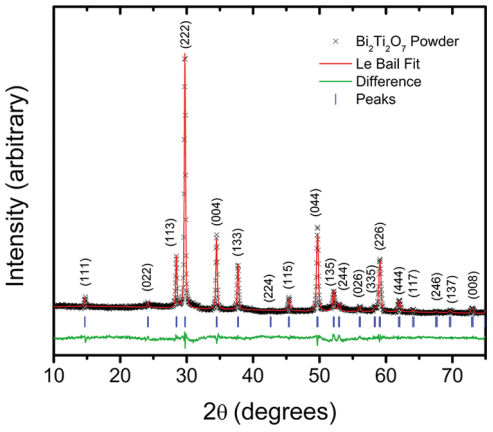

Figure 4. Le Bail structureless fit of the powder XRD pattern. Only peaks ascribed to the pyrochlore phase were detected.

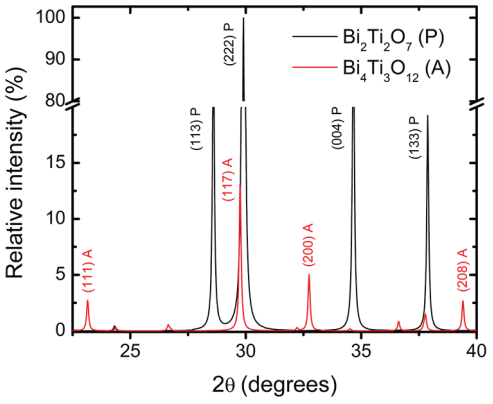

Figure 5. Theoretical XRD pattern of 90 wt % $Bi_2Ti_2O_7$ plus 10 wt % $Bi_4Ti_3O_{12}$.

Masuda et al.[3] worked with the $Bi_2O_3-TiO_2$ system and the flux method to grow single crystals and stated in 1992 that $Bi_2Ti_2O_7$ was part of the phase diagram of the system and its melting point was 1210 °C. Three years later, Kahlenberg and Böhm,[42] determined that the crystal grown by Shidama et al.[41] years before, was actually a different compound. That year (1995) the same authors published another paper[43] in which they tried to make the stoichiometric $Bi_2Ti_2O_7$ by means of solid state reactions. They synthesized a mixture of $Bi_4Ti_3O_{12}$, $Bi_2Ti_4O_{11}$, and the pyrochlore, instead of isolating a single phase. After multiple phase analysis with the Rietveld method, they concluded that the pyrochlore was Bi^{3+} and O^{2-} deficient with a composition of $Bi_{1.833}Ti_2O_{6.75}$ (a = 10.354 Å).

In 1998, Yordanov et al.,[19] claimed the synthesis of $Bi_2Ti_2O_7$ via solid state reactions but no proof (e.g., XRD pattern) was given. The same year, Radosavljevic et al.[39] published for the first time the synthesis of the single phase $Bi_2Ti_2O_7$ obtained with a precipitation method (although very weak peaks of $Bi_2Ti_4O_{11}$ and TiO_2 were still observed in the XRD pattern according to the authors). From neutron diffraction, the compound was identified as $Bi_{1.74}Ti_2O_{6.62}$, with a lattice parameter of 10.352 Å and a density of 6.771 g/cm^3.

In 2002, Hou et al.[16] prepared nanocrystals of $Bi_2Ti_2O_7$ via metallorganic decomposition; however, their XRD pattern clearly shows the presence of the ferroelectric $Bi_4Ti_3O_{12}$ phase. One year later, Su and Lu[20] showed a convincing XRD pattern of a phase pure $Bi_2Ti_2O_7$ made from a sol−gel method. Nonetheless, the complexity of the synthesis method (more than 10 different substances were used through several steps in combination with nitrogen purges and vacuum distillations) described by the authors makes it nonideal for possible applications and in consequence less attractive to researchers. In a latter work (2004), Hector and Wiggin[38] were able to synthesize the compound via coprecipitation. They reported that $Bi_2Ti_2O_7$ was very sensitive to temperature, and therefore, pure phase powder could only be obtained up to 470 °C.

Using the coprecipitation method described in the section 2.1, in this work, phase pure cubic $Bi_2Ti_2O_7$ pyrochlore was successfully synthesized only after calcination at 550 °C. In Figure 2, a comparison between the experimental XRD pattern of the calcined samples and the theoretical pattern obtained from the parameters of Table 1 is presented. It can be noticed that the experimental pattern matches well the prediction from DFT. Additionally, the calculated lattice parameter from the experimental pattern, 10.335 Å ± 0.008 (using a linear extrapolation for curved position-sensitive detectors[40]), is in excellent agreement with the DFT value (10.335 Å ± 0.005).

In addition to the agreement between the XRD patterns in Figure 2, comparing the DFT and experimental patterns shows no unassigned peaks that would be due to the presence of secondary phases. For visual aid, a dashed line was added at 33°, where peaks ascribed to $Bi_4Ti_3O_{12}$ (orthorhombic or tetragonal) and the monoclinic $Bi_2Ti_4O_{11}$ (α or β) would be observed (±0.5°) if any of these phases were present. Again, the absence of peaks associated with the secondary phase(s) and the excellent agreement with the DFT predictions gives strong evidence of the purity of the bismuth titanate pyrochlore. To further illustrate this, a magnification in logarithmic scale of the XRD pattern area around 33° (where impurity peaks would appear if present) is depicted in Figure 3 with dashed lines shown at 33° ± 0.5, and again no sign of impurity peaks is observed. To further verify single-phase purity, a Le Bail refinement (structureless fit) was performed on the powder XRD pattern using the software Rietica. The resulting fit is shown in Figure 4, where it is evident that the sample is composed of a single phase. The small difference between the Le Bail fit and the experimental data corresponds to slight discrepancy in the peak intensities as

expected. The calculated lattice parameter after the refinement was 10.327 Å ± 0.002 (see Table 1). Current efforts are focusing on neutron diffraction to confirm the lattice parameter with higher accuracy and to determine the atomic positions through Rietveld refinement. Particular care will be taken to probe for atomic displacements, especially in the case of Ti which showed unusual displacements in the DFT predictions reported here.

Furthermore, given the pervasive failure to synthesize or isolate phase pure $Bi_2Ti_2O_7$ reported in literature, a detailed description on phase purity identification is presented in the next section.

3.3. Phase Purity Identification of $Bi_2Ti_2O_7$. Single-phase purity is not often reported in literature, since typically the Aurivillius type phase ($Bi_4Ti_3O_{12}$) is present as an impurity. In Figure 5, the theoretical XRD patterns of a mixture composed of 90 wt % $Bi_2Ti_2O_7$ and 10 wt % $Bi_4Ti_3O_{12}$ (structural parameters obtained from Hervoches and Lightfoot[44]) are shown. It is possible to notice that the main peak of the secondary phase, (117)A (near 30°), is overlapped and hidden by the main peak of the pyrochlore, (222)P. Thus, detection of the ferroelectric phase depends on the identification of less intense peaks that even at this relatively high secondary phase concentration are difficult to see. In consequence, low resolution XRD patterns will give the impression of a phase pure compound, when it may not be the case. This could be the reason of the misleading ferroelectricity reports discussed in section 3.6.1.

Figure 6. Phase-pure $Bi_2Ti_2O_7$ powder and pellet.

Perhaps a more practical and direct observation in the identification of the purity of the powder when employing the synthesis method proposed in this work is the color. It was found that the phase pure $Bi_2Ti_2O_7$ powder calcined at 550 °C is white (see Figure 6). With increasing amount of the secondary phases it turns from white to yellow and finally to orange when the concentration of this phases is above 70% (even small amounts as low as 8%, which would be hard to detect via standard XRD, make a big difference in color, as evidenced in Figure 7). Depicted in Figure 6, the phase pure sintered pellets are shown to be light yellow. Since the purity of the pellet was previously established through discussion of Figure 2, it should be noted this difference in color between the pellet and the powder can be explained by the nanosize nature of the latter (it is known that nanoparticles may exhibit different optical properties,[45] for example, gold and silver[46]).

3.4. Phase Stability of $Bi_2Ti_2O_7$. Speranskaya et al.[1] reported in 1965 the presence of only $Bi_4Ti_3O_{12}$ and $Bi_2Ti_4O_{11}$ in the phase diagram of the $Bi_2O_3-TiO_2$ system. Masuda et al.[3] published 27 years later, based on differential thermal analysis, the existence of $Bi_2Ti_2O_7$ in addition to the other two compounds. The three phases were stable in all ranges of temperature up to their incongruent melting points. In recent work, Lopez-Martinez et al.[13] obtained the phase diagram by means of thermodynamic calculations. The results are in agreement with the data obtained experimentally by Masuda et al.[3] However, researchers familiar with $Bi_2Ti_2O_7$ would question the temperature stability. Jiang et al.[17] determined in 1992 that $Bi_2Ti_2O_7$ is an unstable phase since it decomposed to form $Bi_4Ti_3O_{12}$ at 650 °C according to X-ray diffraction analysis. The same result was observed by Toyoda et al.[47] and Nakamura et al.[48] Su and Lu[20] obtained a single $Bi_2Ti_2O_7$ phase and studied the phase transformations at different temperatures. They found that the pyrochlore started to disappear at 700 °C, decomposing to $Bi_4Ti_3O_{12}$ and $Bi_2Ti_4O_{11}$. Hector and Wiggin[38] reported the transition at 480 °C, but it is possible that what they actually saw was not a phase transition, but the crystallization of $Bi_4Ti_3O_{12}$, which might have been present in the sample since the beginning. It should be noted that Speranskaya et al.[1] identified a transformation at 670 °C linking $Bi_4Ti_3O_{12}$ and $Bi_2Ti_4O_{11}$, but did not observe the pyrochlore phase.

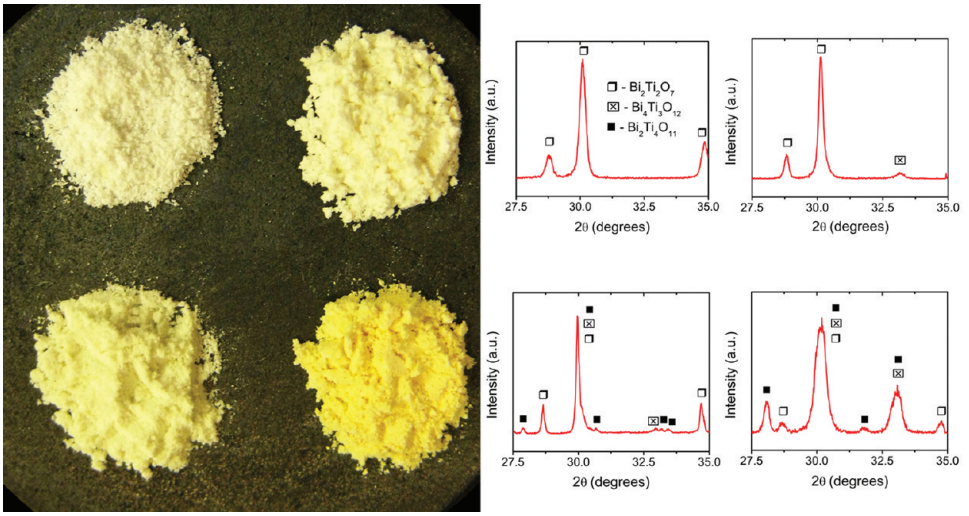

Figure 7. $Bi_2Ti_2O_7$ with 0 wt % (top left), 8 wt % (top right), 50 wt % (bottom left) and >70 wt % (bottom right) of secondary phases. XRD patterns are also shown in the same order.

dx.doi.org/10.1021/cm202154c |Chem. Mater. 2011, 23, 4965–4974

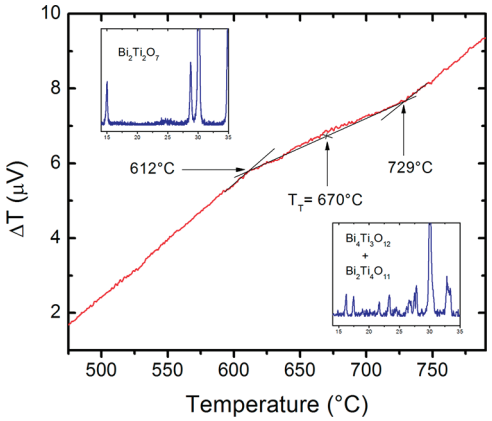

Figure 8. DTA curve of $Bi_2Ti_2O_7$ powder (10 °C/min in nitrogen). The insets correspond to the XRD patterns of the sample below 612 °C (left) and above 729 °C (right).

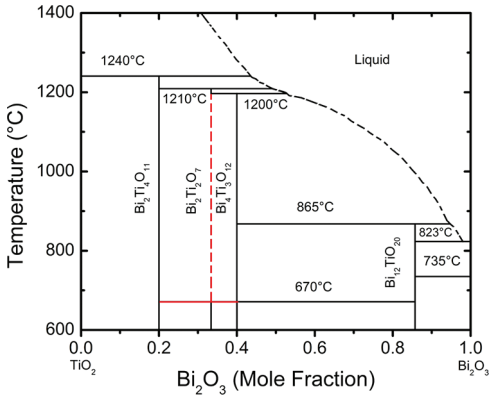

Figure 9. Phase diagram of the Bi_2O_3—TiO_2 system, with modifications (from this work) in red. The horizontal line at 670 °C, absent in recent works, was reinserted and the phase line of $Bi_2Ti_2O_7$ (vertical) was dashed to indicate the thermodynamic instability of this phase.

On the basis of this history of bismuth titanate, it is expected the cubic $Bi_2Ti_2O_7$ will undergo a phase transition at elevated temperature. Therefore, to locate the phase transition temperature of $Bi_2Ti_2O_7$, DTA was performed on the powder. The result shown in Figure 8 reveals the onset of a second-order transition takes place at 612 °C, which extends up to 729 °C, as can be observed from the change in slope of the DTA curve. The absence of a well-defined peak indicates a continuous transition, which explains the difference in the phase transformation temperature observed by different authors. Analysis of the data, like that used for glass transitions (following ASTM E1356), yields a transition temperature of 670 °C. Curiously, it is the same temperature at which $Bi_4Ti_3O_{12}$ starts a phase transformation from orthorhombic to tetragonal.[49] The observed transition in the DTA result demonstrates the need to modify the phase diagram of the Bi_2O_3—TiO_2 system. Accordingly, the phase diagram of Speranskaya et al.[1] based on experimental observations was here combined with the experimental work of Masuda et al.[3] and the thermodynamic predictions of Lopez-Martinez et al.[13] The merged phase diagram with two proposed corrections is shown in Figure 9. First, the horizontal temperature line of 670 °C was reinserted from the $Bi_2Ti_4O_{11}$ phase (0.2 mol fraction Bi_2O_3) to the $Bi_4Ti_3O_{12}$ phase (0.4 mol fraction Bi_2O_3). Second, $Bi_2Ti_2O_7$ phase line at 0.33 mol fraction Bi_2O_3 from 670 to 1200 °C was dashed to indicate the thermodynamic instability (and dependence on processing history) of the pyrochlore phase.

3.5. Sintering of $Bi_2Ti_2O_7$. Obtaining large single crystals or a dense polycrystalline ceramics is essential for determining key bulk thermophysical and electrical properties of $Bi_2Ti_2O_7$. Unfortunately, until now, it is precisely the instability of the pyrochlore phase that has impeded the successful growth of large single crystals or the sintering of the compound. The consequence has been the inaccurate determination of properties, such as dielectric.[50] This is one of the reasons why most of the interest has shifted to the study of thin films prepared with different methods.[51−59] However, the key to solving the sintering issue was found in the revised phase diagram presented in Figure 9. As discussed in section 3.4, the $Bi_2Ti_2O_7$ phase is stable up to 670 °C. This effectively precludes the use of any conventional sintering method. However, recognizing that the phase diagram represents thermodynamic equilibrium, it should be possible, in principle, to heat the pyrochlore rapidly to 1200 °C (or near the appearance of liquid) to move away from thermal equilibrium and prevent the formation of the more stable secondary phases above 670 °C. Such process of sintering kinetics enhancement while limiting the phase transformation kinetics obviously requires very fast heating rates.

The necessary heating rates were achieved by microwave sintering (80 °C/min), which exposed the pellets to 1200 °C within 15 min. The obtained density (measured by the Archimedes method) was 6.93 g/cm^3. This would correspond to roughly 92% of the theoretical density, 7.53 g/cm^3 (assuming a fully stoichiometric compound). The XRD pattern of the pellet is presented in Figure 2. It matches well the theoretical and powder patterns. The lack of additional peaks near the dashed line in Figure 2 indicates the secondary phases are not present in the sintered pellet.

It is important to note that since liquid phase appears at 1210 °C according to the phase diagram of Figure 9, there is a very small working window to achieve a sintered pellet and small fluctuations can affect the desired outcome. For example, it is clear that even if small amounts of the pyrochlore melt, it would lead to the formation of $Bi_2Ti_4O_{11}$ because of the peritectic reaction. In addition, a sintering temperature of 1150 °C resulted in gray pellets with a density of 6.63 g/cm^3 for which XRD analysis revealed the presence of only $Bi_4Ti_3O_{12}$ and $Bi_2Ti_4O_{11}$ as expected.

Furthermore, it is clear that, starting with nanometer sized powder, which coprecipitation yields, is essential to maximize the driving force for sintering (surface area) and obtaining a dense polycrystalline ceramic. Therefore, details on the powder morphology and sintered ceramic are provided in the following subsection.

3.5.1. Powder Morphology and Ceramic Microstructure Analysis. To study the powder morphology and ceramic microstructure, SEM images were collected. As can be noticed from Figure 10a, the powder obtained from the coprecipitation method is comprised of round 100 nm clusters (hard agglomerates) of smaller ~15 nm particles. Figure 10b (at lower magnification) also shows that these clusters result in powder of homogeneous round shape with very few soft agglomerates, this also very important to ensure the densification of the ceramic. Given the fast firing employed, after sintering, no grain growth was observed as can be inferred from the fractured pellet (under bending) of Figure 10c. Additional confirmation was observed in a lower magnification image (Figure 10d) that showed the homogeneous grain distribution of the sample. The effective

dx.doi.org/10.1021/cm202154c |*Chem. Mater.* 2011, 23, 4965–4974

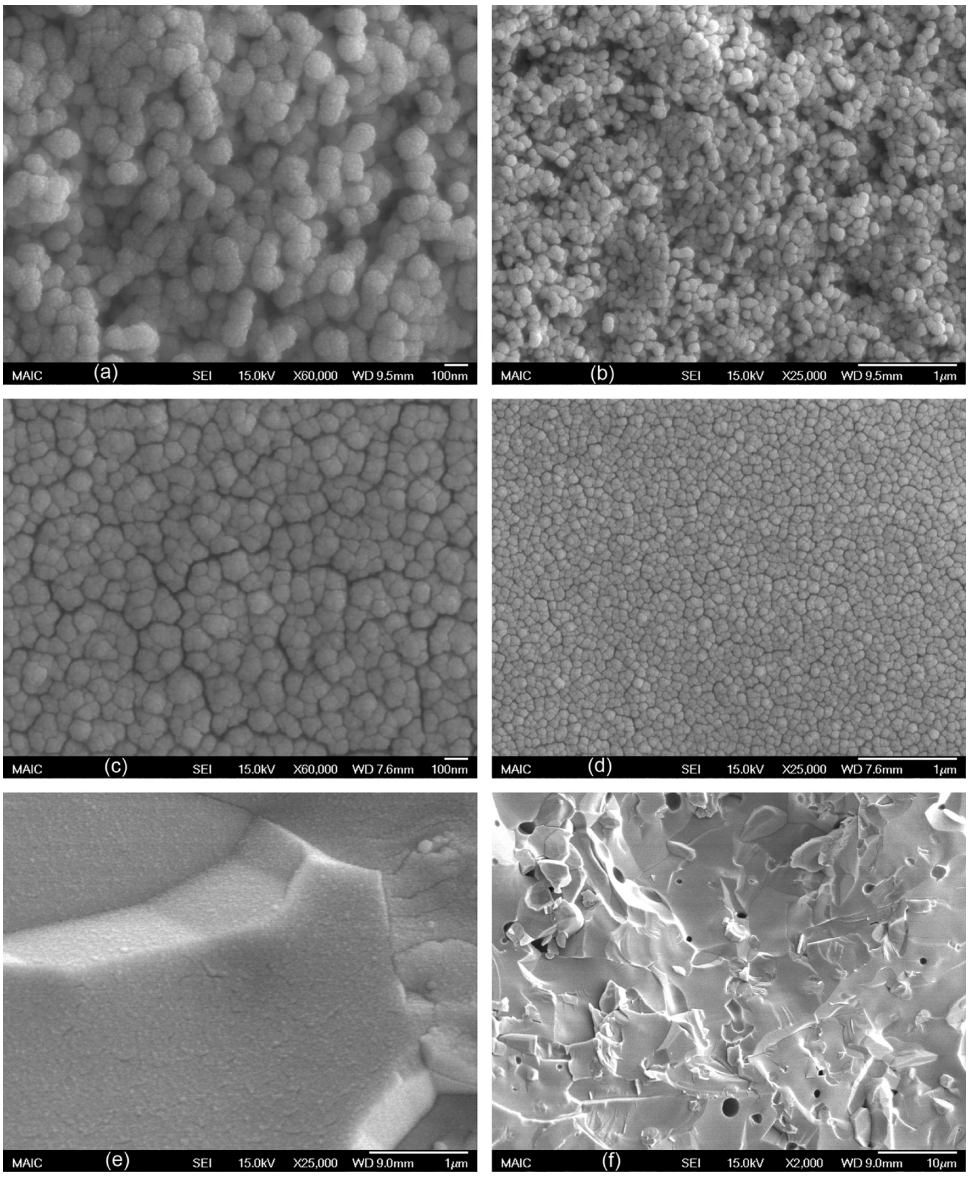

Figure 10. SEM images of the powder (a,b), and fracture surfaces under bending (c,d) and shearing (e,f).

conservation of the nanograins has been previously observed in microwave sintering.[60,61] The image of the surface of a pellet fractured under shear stress is presented in Figure 10e and reveals a transgranular fracture with a compacted structure where the nanograins cannot be easily differentiated, unlike the case in Figure 10d. At a lower magnification, Figure 10f exhibits the dense nature of the pellet but also illustrates the presence of some isolated porosity.

3.6. $Bi_2Ti_2O_7$ Electrical Properties. *3.6.1. Polarization vs Electric Field Loop Behavior.* The believed ferroelectricity of $Bi_2Ti_2O_7$ has been especially controversial. Several authors have published this supposed characteristic of $Bi_2Ti_2O_7$,[3,15−19] but on the other hand, the compound has been reported as a cubic pyrochlore,[38,39,41] thereby ruling out the possibility of a ferroelectric behavior. Moreover, Su and Lu[20] did not find the hysteresis loop characteristic of the ferroelectric materials but a single line. In addition, the DFT calculations previously discussed predict a cubic structure. Therefore, the obtained sintered pellets of phase pure $Bi_2Ti_2O_7$ reported here are ideal to help clarify the disagreement.

In Figure 11, the polarization versus electric field response obtained for $Bi_2Ti_2O_7$ is illustrated. Clearly no ferroelectricity was observed and the small loop, which does not exhibit concave regions, was understandably ascribed to dielectric loss. It is important to note that incorrect data interpretation has led to at least one report of ferroelectric behavior of $Bi_2Ti_2O_7$ when it was clearly not the case[18] (for more information regarding proper identification of ferroelectrics from hysteresis loops, please refer to the work by Scott[62]). More importantly, the calculated relative permittivity from the polarization and the electric field at 50 Hz and room temperature was ∼162 (see eq 1). As will be seen in the next section, this matches very well with the dielectric permittivity of $Bi_2Ti_2O_7$ here measured.

$$\varepsilon_r = \left(\frac{P}{E\varepsilon_0}\right) + 1 \qquad (1)$$

dx.doi.org/10.1021/cm202154c |*Chem. Mater.* 2011, 23, 4965–4974

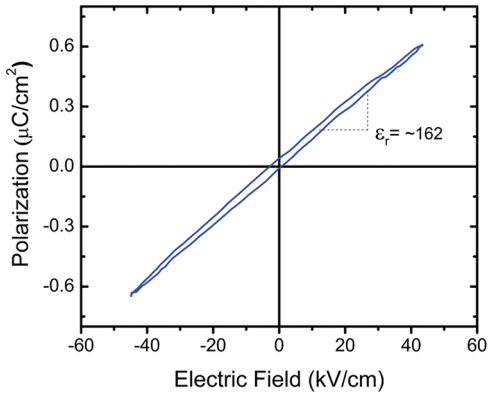

Figure 11. Polarization vs electric field response of $Bi_2Ti_2O_7$ measured with a Sawyer−Tower circuit at 50 Hz.

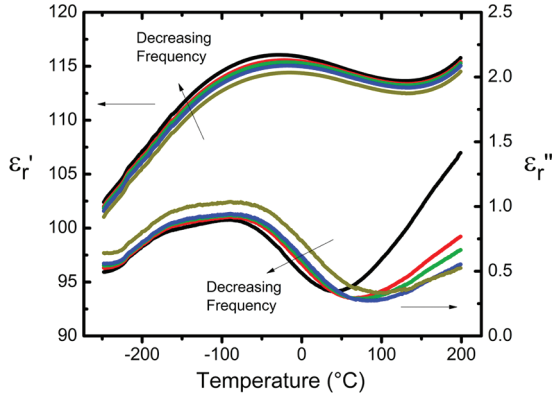

Figure 12. Dielectric permittivity of $Bi_2Ti_2O_7$ as a function of temperature from 500 to 2000 kHz.

where ε_r is the relative permittivity, P is the polarization, E is the electric field, and ε_o is the permittivity of vacuum.

3.6.2. Dielectric properties. Bismuth pyrochlores have desirable dielectric properties, including high dielectric constant, low dielectric loss, and low temperature coefficients of capacitance which help to decrease the size of the capacitors, as well as lower the material costs. In fact, bismuth titanate was combined with bismuth hafnate to form solid solutions in an effort to improve the overall dielectric properties.[50] Another example of this is BZN ($Bi_{1.5}Zn_{0.92}Nb_{1.5}O_{6.92}$) which also shows dielectric relaxation.[63] The dielectric relaxation observed in pyrochlores is often attributed to multiple features such as the highly polarizable A site cation, chemical substitution, and large ion displacement from the ideal $Fd\bar{3}m$ (space group No. 227) sites of the cubic pyrochlore structure.[64,65] The sintered phase-pure $Bi_2Ti_2O_7$ pellet presents an opportunity to understand the dielectric properties of a pyrochlore without the chemical substitution on the A or B site, thereby helping to isolate the features necessary to observe dielectric relaxation. The dielectric behavior of $Bi_2Ti_2O_7$ was investigated and the results are presented in Figure 12. The dielectric constant of 115 at 500 kHz and room temperature is relatively high and the dielectric loss is small with the imaginary part of the permittivity <1 (i.e., tan δ < 0.01).

The permittivity indirectly calculated from the hysteresis loop at room temperature and 50 Hz (presented in Figure 11) is in good agreement with the direct measurements in Figure 12 when considering that the permittivity increases with decreasing frequency, as expected. Further, although it is not included in Figure 12, at 1 kHz the permittivity was 128. More remarkably, it is clear that bismuth titanate exhibits a form of dielectric relaxation commonly observed in pyrochlores.[63,65−68] In a typical bismuth pyrochlore relaxation, the maxima in the real part of the dielectric permittivity (ε_r') is relatively sharp and the curves at different frequencies tend to converge at higher temperature to the same permittivity value. As seen in Figure 12, for bismuth titanate this behavior is not exactly followed. Instead, the curves remain separated and the peak in permittivity is softened. The shape of the associated dielectric loss peak is rather interesting and deserves further investigation since it does not follow the typical peak from relaxation processes. Nonetheless, inspection of ε_r'' in Figure 12 does reveal similar features to the other pyrochlores. Specifically, a shift of T_m (temperature at which the peak in the dielectric loss curve occurs) to higher temperatures with increasing frequency, and the increment of the loss when the frequency is higher. Therefore, it is clear that dielectric relaxation is observed in $Bi_2Ti_2O_7$, confirming the suggestion by Cagnon et al.[51] that the negligible tunability of $Bi_2Ti_2O_7$ thin films may be due to a dielectric relaxation.

Additionally, recent computational work examining atomic hopping mechanisms in bismuth titanate suggested the occurrence of dielectric relaxation due to Bi/O′ transitioning between equivalent displacement positions.[31] The observation of dielectric relaxation in bismuth titanate suggests of the multiple features proposed to be necessary, atomic displacement is key. Clearly, further investigation of the nature of the dielectric response of bismuth titanate is needed and it is the focus of current investigations. The results will further help in providing insights about the dielectric behavior of this and other pyrochlore compounds.[63,65−68]

4. CONCLUSIONS

Cubic pyrochlore $Bi_2Ti_2O_7$ was synthesized by a coprecipitation route. The powder was microwave sintered at 1200 °C to avoid the formation of the thermodynamically more favorable secondary phases, $Bi_4Ti_3O_{12}$ and $Bi_2Ti_4O_{11}$. The XRD pattern of the compound, also modeled by DFT, confirmed the phase purity of both, the powder and the densified ceramic. It was clarified that given the difficulty in making a single phase of the pyrochlore structure, properties have been incorrectly ascribed to this compound (e.g., ferroelectricity). To help researchers avoid confusions of this sort, a brief description of how to identify the presence of impurities based on the color of the powder was offered. In addition, theoretical X-ray diffraction patterns were shown to explain why the ferroelectric $Bi_4Ti_3O_{12}$ commonly goes unnoticed in the experimental patterns, which is a possible reason of the misleading properties attributed to $Bi_2Ti_2O_7$. The cubic pyrochlore is not a ferroelectric as proven by the polarization vs electric field response of the sintered pellets made here. The relative permittivity of ∼162, calculated from the slope of the hysteresis loop, is in good agreement with the results obtained from the dielectric measurements, from which dielectric relaxation was observed. The fact that this phenomenon takes place in a pyrochlore with no substitution on the A or B site, strongly suggests, altogether with recent computational work, that atomic displacements from the high symmetry sites is sufficient condition for the appearance of dielectric relaxation behavior in bismuth pyrochlores.

■ ASSOCIATED CONTENT

Supporting Information. Crystallographic information file (CIF) of $Bi_2Ti_2O_7$, based on the DFT simulations. This material is available free of charge via the Internet at http://pubs.acs.org.

■ AUTHOR INFORMATION

Corresponding Author
*E-mail: jnino@mse.ufl.edu.

■ ACKNOWLEDGMENT

This work is supported partially by the U.S. National Science Foundation under grants DMR 0449710 and CBET 0730900. The authors want to thank Cassandra Llano and Prof. Jacob Jones for assistance with the ferroelectric measurements, and the assistance of Dr. Jennifer S. Forrester on the use of the software Rietica. In addition, the aid of Dr. Wei Qiu, Dr. Terrell A. Vanderah, Dr. Andrew L. Hector, and Christopher G. Turner during the initial attempts to synthesize the bismuth titanate compound is greatly appreciated. Finally, the Major Analytical Instrumentation Center of the University of Florida for providing access to the SEM is recognized.

■ REFERENCES

(1) Speranskaya, E. I.; Rez, I. S.; Kozlova, L. V.; Skorikov, V. M.; Slavov, V. I. *Neorg. Mater.* **1965**, *1*, 232.
(2) Bruton, T. M. *J. Solid State Chem.* **1974**, *9*, 173.
(3) Masuda, Y.; Masumoto, H.; Baba, A.; Goto, T.; Hirai, T. *Jpn. J. Appl Phys 1* **1992**, *31*, 3108.
(4) Morozov, M. I.; Mezentseva, L. P.; Gusarov, V. V. *Russ J Gen Chem* **2002**, *72*, 1038.
(5) Pookmanee, P.; Boonphayak, P.; Phanichphant, S. *Ceram. Int.* **2004**, *30*, 1917.
(6) Alguero, M.; Ferrer, P.; Vila, E.; Iglesias, J. E.; Castro, A. *J. Am. Ceram. Soc.* **2006**, *89*, 3340.
(7) Kahlenberg, V.; Bohm, H. *J. Phys.: Condens. Mater.* **1994**, *6*, 6211.
(8) Kahlenberg, V.; Bohm, H. *Acta Crystallogr. B* **1995**, *51*, 11.
(9) Zhou, J. K.; Zou, Z. G.; Ray, A. K.; Zhao, X. S. *Ind. Eng. Chem. Res.* **2007**, *46*, 745.
(10) Thanabodeekij, N.; Gulari, E.; Wongkasemjit, S. *Powder Technol.* **2005**, *160*, 203.
(11) Carvalho, J. F.; Hernandes, A. C. *J. Cryst. Growth* **1999**, *205*, 185.
(12) Okano, Y.; Wada, H.; Fukuda, T.; Miyazawa, S. *Jpn. J. Appl. Phys. 2* **1991**, *30*, L1307.
(13) Lopez-Martinez, J.; Romero-Serrano, A.; Hernandez-Ramirez, A.; Zeifert, B.; Gomez-Yanez, C.; Martinez-Sanchez, R. *Thermochim. Acta* **2011**, *516*, 35.
(14) Knop, O.; Brisse, F. *Can. J. Chem.* **1969**, *47*, 971.
(15) Hou, Y.; Huang, Z. M.; Xue, J. Q.; Wu, Y. N.; Shen, X. M.; Chu, J. H. *Appl. Phys. Lett.* **2005**, 86.
(16) Hou, Y.; Wang, M.; Xu, X. H.; Wang, D.; Wang, H.; Shang, S. X. *J. Am. Ceram. Soc.* **2002**, *85*, 3087.
(17) Jiang, A. Q.; Hu, Z. X.; Zhang, L. D. *J. Appl. Phys.* **1999**, *85*, 1739.
(18) Kim, S. S.; Park, M. H.; Chung, J. K.; Kim, W. J. *J. Appl. Phys.* **2009**, 105.
(19) Yordanov, S. P.; Ivanov, I.; Carapanov, C. P. *J. Phys. D: Appl. Phys.* **1998**, *31*, 800.
(20) Su, W. F.; Lu, Y. T. *Mater. Chem. Phys.* **2003**, *80*, 632.
(21) Kresse, G.; Furthmüller, J. *Comput. Mater. Sci.* **1996**, *6*, 15.
(22) Kresse, G.; Furthmüller, J. *Phys. Rev. B* **1996**, *54*, 11169.
(23) Kresse, G.; Hafner, J. *Phys. Rev. B* **1993**, *47*, 558.
(24) Kresse, G.; Hafner, J. *Phys. Rev. B* **1994**, *49*, 14251.
(25) Blöchl, P. E. *Phys. Rev. B* **1994**, *50*, 17953.
(26) Kresse, G.; Joubert, D. *Phys. Rev. B* **1999**, *59*, 1758.
(27) Kohn, W.; Sham, L. J. *Phys. Rev.* **1965**, *140*, A1133.
(28) Hinojosa, B. B.; Nino, J. C.; Asthagiri, A. *Phys. Rev. B* **2008**, *77*, 104123.
(29) Pruneda, J. M.; Artacho, E. *Phys. Rev. B* **2005**, *72*, 085107.
(30) Methfessel, M.; Paxton, A. T. *Phys. Rev. B* **1989**, *40*, 3616.
(31) Hinojosa, B. B.; Asthagiri, A.; Nino, J. C. *Appl. Phys. Lett.* **2011**, *99*, 082903.
(32) Monkhorst, H. J.; Pack, J. D. *Phys. Rev. B* **1976**, *13*, 5188.
(33) Fennie, C.; Seshadri, R.; Rabe, K. *arXiv:0712.1846* 2008, unpublished.
(34) Hinojosa, B. B.; Lang, P. M.; Asthagiri, A. *J. Solid State Chem.* **2010**, *183*, 262.
(35) Patterson, C. H. *Phys. Rev. B* **2010**, *82*, 155103.
(36) Seshadri, R. *Solid State Sci.* **2006**, *8*, 259.
(37) Shoemaker, D. P.; Seshadri, R.; Hector, A. L.; Llobet, A.; Proffen, T.; Fennie, C. J. *Phys. Rev. B* **2010**, *81*, 144113.
(38) Hector, A. L.; Wiggin, S. B. *J. Solid State Chem.* **2004**, *177*, 139.
(39) Radosavljevic, I.; Evans, J. S. O.; Sleight, A. W. *J. Solid State Chem.* **1998**, *136*, 63.
(40) Pramanick, A.; Jones, J. L.; Omar, S.; Nino, J. C. *J. Appl. Crystallogr.* **2009**, *42*, 490.
(41) Shimada, S.; Kodaira, K.; Matsushita, T. *J. Cryst. Growth* **1977**, *41*, 317.
(42) Kahlenberg, V.; Bohm, H. *J. Alloys Compd.* **1995**, *223*, 142.
(43) Kahlenberg, V.; Bohm, H. *Cryst Res Technol* **1995**, *30*, 237.
(44) Hervoches, C. H.; Lightfoot, P. *Chem. Mater.* **1999**, *11*, 3359.
(45) Bohren, C.; Huffman, D. *Absorption and Scattering of Light by Small Particles*; Wiley-VCH: Mörlenbach, Germany, 1998.
(46) Sun, Y.; Xia, Y. *Analyst* **2003**, *128*, 686.
(47) Toyoda, M.; Hamaji, Y.; Tomono, K.; Payne, D. A. *Jpn. J. Appl. Phys.* **1993**, *32*, 4158.
(48) Nakamura, T.; Muhammet, R.; Shimizu, M.; Shiosaki, T. *Jpn. J. Appl. Phys.* **1993**, *32*, 4086.
(49) Zhou, Q. D.; Kennedy, B. J.; Howard, C. J. *Chem. Mater.* **2003**, *15*, 5025.
(50) Henderson, S. J.; Shebanova, O.; Hector, A. L.; McMillan, P. F.; Weller, M. T. *Chem. Mater.* **2007**, *19*, 1712.
(51) Cagnon, J.; Boesch, D. S.; Finstrom, N. H.; Nergiz, S. Z.; Keane, S. P.; Stemmer, S. *J. Appl. Phys.* **2007**, 102.
(52) Fu, L. W.; Wang, H.; Shang, S. X.; Wang, X. L.; Xu, P. M. *J. Cryst. Growth* **1994**, *139*, 319.
(53) Kidchob, T.; Malfatti, L.; Marongiu, D.; Enzo, S.; Innocenzi, P. *J. Am. Ceram. Soc.* **2010**, *93*, 2897.
(54) Suzuki, M.; Watanabe, T.; Takenaka, T.; Funakubo, H. *J. Eur. Ceram. Soc.* **2006**, *26*, 2155.
(55) Wang, J. C.; Yang, C. H.; Hu, G. D.; Wu, W. B.; Cheng, L.; Chen, X. M. *J. Alloys Compd.* **2010**, *494*, 285.
(56) Wang, S. W.; Lu, W.; Li, N.; Li, Z. F.; Wang, H.; Wang, M.; Shen, X. C. *Mater. Res. Bull.* **2002**, *37*, 1691.
(57) Wang, S. W.; Wang, H.; Shang, S. X.; Huang, J.; Wang, Z.; Wang, M. *J. Cryst. Growth* **2000**, *217*, 388.
(58) Wang, S. W.; Wang, H.; Wu, X. M.; Shang, S. X.; Wang, M.; Li, Z. F.; Lu, W. *J. Cryst. Growth* **2001**, *224*, 323.
(59) Wu, X. M.; Wang, S. W.; Wang, H.; Wang, Z.; Shang, S. X.; Wang, M. *Thin Solid Films* **2000**, *370*, 30.
(60) Das, S.; Mukhopadhyay, A. K.; Datta, S.; Basu, D. *Bull. Mater. Sci* **2009**, *32*, 1.
(61) Ramesh, S.; Tan, C. Y.; Bhaduri, S. B.; Teng, W. D. *Ceram. Int.* **2007**, *33*, 1363.
(62) Scott, J. F. *J. Phys.: Condens. Matter* **2008**, *20*, 021001.
(63) Nino, J. C.; Lanagan, M. T.; Randall, C. A. *J. Appl. Phys.* **2001**, *89*, 4512.
(64) Levin, I.; Amos, T. G.; Nino, J. C.; Vanderah, T. A.; Randall, C. A.; Lanagan, M. T. *J. Solid State Chem.* **2002**, *168*, 69.

(65) Roth, R. S.; Vanderah, T. A.; Bordet, P.; Grey, I. E.; Mumme, W. G.; Cai, L.; Nino, J. C. *J. Solid State Chem.* **2008**, *181*, 406.
(66) Vanderah, T. A.; Lufaso, M. W.; Adler, A. U.; Levin, I.; Nino, J. C.; Provenzano, V.; Schenck, P. K. *J. Solid State Chem.* **2006**, *179*, 3467.
(67) Ang, C.; Yu, Z.; Youn, H. J.; Randall, C. A.; Bhalla, A. S.; Cross, L. E.; Nino, J.; Lanagan, M. *Appl. Phys. Lett.* **2002**, *80*, 4807.
(68) Wang, H.; Kamba, S.; Du, H. L.; Zhang, M. L.; Chia, C. T.; Veljko, S.; Denisov, S.; Kadlec, F.; Petzelt, J.; Yao, X. *J. Appl. Phys.* **2006**, 100.